Ordering in fcc lattices with first- and second-neighbor interactions

J. M. Sanchez and D. de Fontaine
*Materials Department, University of California, Los Angeles, California 90024**
(Received 19 January 1979)

A prototype phase diagram for the $\langle 1\frac{1}{2}0\rangle$ family of the ordered superstructures in fcc lattices is calculated in the tetrahedron-octahedron approximation of the cluster variation method. The tetrahedron-octahedron cluster combination allows for first- and second-neighbor interactions, both essential for the $\langle 1\frac{1}{2}0\rangle$ superstructures to be ground states. Calculations are carried out for positive (antiferromagnetic) nearest-neighbor pair interactions and for a ratio of second- to first-neighbor interaction energies of 0.25. Salient features of the resulting phase diagram are tricritical points in the fcc to A_2B_2 and the fcc to A_3B transitions, and the presence of a bicritical point at the junction of the A_2B_2 and A_3B critical lines with the A_2B_2 to A_3B first-order transition line. The A_2B phase of the $\langle 1\frac{1}{2}0\rangle$ family is found to be stable at relatively low temperatures and in a very narrow composition range. Stability of the disordered state is investigated in k space and the $\langle 1\frac{1}{2}0\rangle$ ordering spinodal is determined.

I. INTRODUCTION

The cluster variation method (CVM),[1] which has been used successfully to treat a wide range of phase-transformation phenomena, has recently been applied to the calculation of equilibrium phase diagrams. In particular, Van Baal[2] calculated the phase diagram for an fcc antiferromagnetic spin-$\frac{1}{2}$ Ising model in the so-called tetrahedron approximation of the CVM. Such Ising model is isomorphic to a binary alloy with only nearest-neighbors (nn) interactions. Notwithstanding intrinsic deficiencies of the Ising model for treating real binary alloys, Van Baal's calculation showed general qualitative agreement with the CuAu system. Subsequently, de Fontaine and Kikuchi,[3,4] by including many-body interactions in the tetrahedron approximation have been able to reproduce the CuAu solid-state phase diagram with remarkable closeness.

Despite such unquestionable success, the tetrahedron approximation is seriously limited by the form of the internal energy: it can only contain nn pair interactions and many-body interactions associated to the nn equilateral triangle and to the nn regular tetrahedron. It is well known that, in the event of only nn pairs interactions, the ground states, i.e., the stochiometric ordered structures with the lowest energy, are degenerate.[5-7] Furthermore, the degeneracy is not lifted by including many-body interactions which are allowed by the approximation (tetrahedron).[8]

Degeneracy of ground states generally poses difficulties since, when using the CVM, sublattices must be introduced *a priori* in order to treat a given ordered structure. Thus, all ground-state structures, degenerate or otherwise, should in principle be investigated. For example, when calculating the CuAu phase diagram in the tetrahedron approximation, it is proper to ask whether the model predicts the $L1_2$ (Cu_3Au) or the $D0_{22}$ (Ni_3V) structures, with the same ground-state energy, to be the stable ordered phases. From a more practical point of view, however, the main drawback of the tetrahedron approximation is that it can treat a very limited number of fcc ordered structures, namely, those of the $\langle 100\rangle$ family (see below).

The object of this investigation is to establish a free-energy model which will describe a wider range of fcc ordered structures than heretofore possible with the tetrahedron approximation. In doing so, it is essential to determine the ground states for a given energy model since these dictate the type of ordered superstructures that can eventually be found to be stable phases in a CVM calculation.

The ground-state problem in the case of an fcc lattice with nn and next-nearest-neighbors (nnn) pair interactions has been completely solved[5-7] and a partial list of ground-state structures for the case of up to fourth-neighbor interactions has recently been derived by Kanamori.[7] It is interesting to note that a simple energy model including nn and nnn interactions accounts for a large number of observed fcc ordered superstructures, whereas most of the ground states which appear as a consequence of fourth-neighbor interactions have not been observed experimentally. Thus, without increasing the level of complexity much beyond the tetrahedron approximation, we can expect to have a realistic free-energy model by only including nn and nnn interactions.

For an antiferromagnetic (ordering, i.e., positive)

nn interaction energy v_1, three cases can be distinguished, depending on the ratio $\alpha = v_2/v_1$, where v_2 is the nnn interaction energy. These three cases are conveniently classified in terms of families of ordered structures labeled by the point in k space where the Fourier transform of the pairwise energy has its absolute minimum.[9] Such families are: (i) the $\langle 100 \rangle$ family for $\alpha < 0$, (ii) $\langle \frac{1}{2}\frac{1}{2}\frac{1}{2} \rangle$ family for $\alpha > \frac{1}{2}$, and (iii) the $\langle 1\frac{1}{2}0 \rangle$ family for $0 < \alpha < \frac{1}{2}$. The ground-state ordered superstructures belonging to each family are summarized in Table I where the space group and, when applicable, the structure information and examples are given.[5–7,10] In this work, we will solely concentrate in some ordered structures of the $\langle 1\frac{1}{2}0 \rangle$ family.

As seen in Table I, the $\langle 1\frac{1}{2}0 \rangle$ family comprises six different ordered structures. At stochiometry $\frac{1}{3}$, there are three different degenerate structures: A_2B, A_2B', and A_2B'' (see Table I). The A_2B' and A_2B'' structures together with that of the A_5B phase at stoichiometry $\frac{1}{6}$, have monoclinic Bravais lattices.[7]

Calculations will be carried out for the following ground-state superstructures of the $\langle 1\frac{1}{2}0 \rangle$ family: (i) the A_2B_2 phase with space group $I4_1/amd$, (ii) the A_2B phase with space group $Immm$, and (iii) the A_3B phase with space group $I4/mmm$. The three structures above have a particularly simplifying feature in common: they can be formally obtained by stacking of (420) lattice planes which are either occupied by A or by B atoms.[11] On the other hand, the remaining $\langle 1\frac{1}{2}0 \rangle$ superstructures, namely, the monoclinics A_2B', A_2B'', and A_5B cannot be obtained by stacking of pure A or B (420) planes. Due to the fact that low symmetry makes actual computations a cumbersome undertaking and that the structures in question do not seem to be realized in nature, we will not consider them further in this work. The particular sequences of planes for the A_2B_2, A_2B, and A_3B superstructures are schematically shown in Fig. 1 together with a (001) projection of their respective unit cells. The representation introduced by Kanamori[7] has been used here: large circles are on a given (001) plane and small circles in the planes immediately above or below; the components A and B are represented by open and shaded circles, respectively.

Included in Fig. 1 is the $D1a$ structure with stochiometry 1/5 (A_4B) and space group $I4/m$. The $D1a$ structure, an example of which is Ni_4Mo, is not a ground state in the nn and nnn energy model used here, but it is degenerate with a mixture of the A_3B ($D0_{22}$) and the monoclinic A_5B phases of the $\langle 1\frac{1}{2}0 \rangle$ family.[6,7] Nonetheless, the A_4B phase was included in our study since it can also be obtained by stacking pure A or B (420) planes. Anticipating the results of Sec. IV, we may mention here that the A_4B phase was found to be unstable for the particular value of nnn to nn interaction-energy ratio of 0.25 and temperature range used in our calculations. Such finding clearly emphasizes the importance of a detailed analysis of the ground-state problem previous to CVM calculations.

II. CONFIGURATIONAL FREE ENERGY

The free energy of a crystalline system composed of different atomic species, say A and B for binaries, is obtained, in the CVM, by minimizing the functional F

$$F = \langle E \rangle - k_B T \ln \Omega \ , \tag{1}$$

TABLE I. Ground states for the fcc lattice with nn (v_1) and nnn (v_2) pair interactions. For $v_1 > 0$, three families are observed depending on the ratio $\alpha = v_2/v_1$.

α	Family	Formula	"Structurbericht" symbol	Symmetry class	Int. table	Examples
$\alpha < 0$	$\langle 100 \rangle$	AB	$L1_0$	s. tetragonal	$P4/mmm$	CuAu I
		A_3B	$L1_2$	s. cubic	$Pm3m$	Cu_3Au
$\alpha > 0.5$	$\langle \frac{1}{2}\frac{1}{2}\frac{1}{2} \rangle$	AB	$L1_1$	rhombohedral	$R\bar{3}m$	CuPt
		A_2B	...	sc monoclinic	$B2/m$	...
$0 < \alpha < 0.5$	$\langle 1\frac{1}{2}0 \rangle$	A_2B_2	...	bc tetragonal	$I4_1/amd$	...
		A_2B	...	bc orthorhombic	$Immm$	Pt_2Mo, Ni_2V
		A_2B'	...	sc monoclinic	$B2/m$	...
		A_2B''	...	sc monoclinic	$B2/m$	...
		A_3B	$D0_{22}$	bc tetragonal	$I4/mmm$	Ni_3V, Al_3Ti
		A_5B	...	sc monoclinic	$B2/m$	...

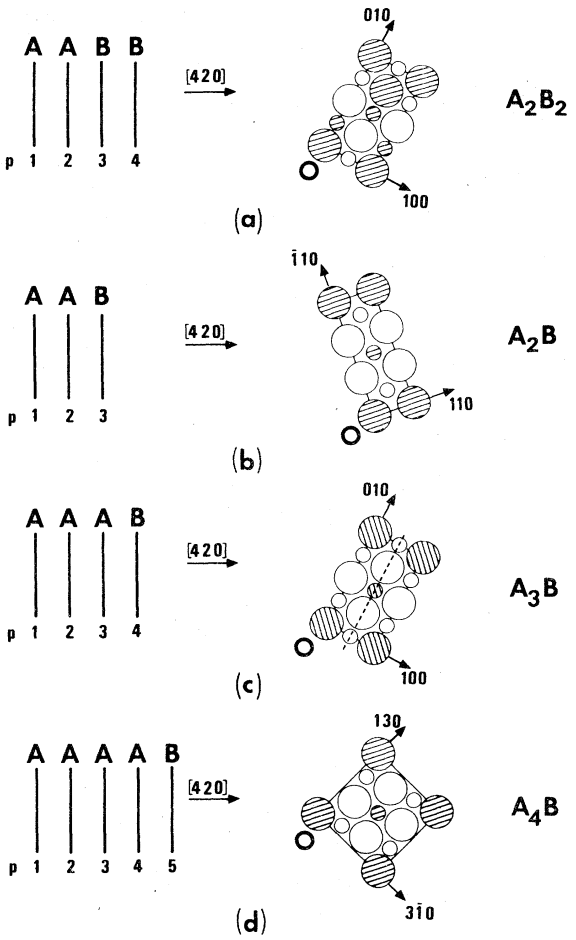

FIG. 1. Projection on a (001) plane of the unit cells and stacking sequence of (420) planes for the (a) A_2B_2; (b) A_2B; (c) A_3B; and (d) A_4B superstructures of the fcc lattice. Open and filled circles correspond to A and B atoms, respectively. Large circles are on a (001) plane and small ones on the planes immediately above or below.

where Ω stands for the number of configurations of the crystal lattice, i.e., arrangements of A and B atoms, having the same average value $\langle E\rangle$ of the configurational energy.[1]

Different levels of approximations of the CVM are obtained by including successively larger clusters in the calculation of the number of configurations Ω. Due to practical computational difficulties, however, most of the CVM calculations have been confined to relatively small cluster sizes. It was only recently that approximations allowing for higher-neighbor interactions, although applied to the simple case of the Ising ferromagnet, have been studied.[12,13]

A suitable choice of clusters for calculating the phase diagram for the $\langle 1\frac{1}{2}0\rangle$ family of fcc ordered structures is a combination of the regular octahedron, including nn and nnn, and the regular nn tetrahedron.[12,13] This octahedron-tetrahedron (O-T) approximation is particularly reliable, yielding a ferromagnetic critical temperature for the fcc Ising model only 2% higher than the best present estimate.[12,13] In the O-T approximation, we can lift the degeneracy between the $\langle 100\rangle$, $\langle\frac{1}{2}\frac{1}{2}\frac{1}{2}\rangle$, and $\langle 1\frac{1}{2}0\rangle$ families by including the essential nn and nnn pair interactions (v_1 and v_2) referred to in the Introduction.

In terms of the spin operator $\sigma(r)$, which takes values $+1$ or -1 if lattice point r is, respectively, occupied by an A or B atom, we can write the configuration energy E of the system

$$E=\tfrac{1}{2}v_1\sum_r\sum_{r_1}\sigma(r)\sigma(r+r_1)+\tfrac{1}{2}v_2\sum_r\sum_{r_2}\sigma(r)\sigma(r+r_2)\ , \tag{2}$$

where the sums over r are over all lattice points, and where those over r_1 and r_2 are, respectively, over all nn and nnn to r.

The quantity of interest is the average value of the energy as indicated by the angular brackets in Eq. (1). Such brackets refer to an ensemble average which, in general, depends on the space-group symmetry of the phase under consideration. That is, in order to treat a given ordered phase in the CVM, it is necessary to introduce a set of sublattices which, for the purpose of computing averages, must be properly distinguished.

In principle, it is possible to associate a distinct sublattice with each lattice point in the crystal,[11] thus allowing us to treat any arbitrary ordered structure based on the parent disordered lattice. This approach will be shown (Sec. III) to be particularly useful for the treatment of instabilities in k space. For the actual computation of the phase diagram a finite number of sublattices will be obtained for each phase by applying the symmetry operations of the associated space group. Note that for those members of the $\langle 1\frac{1}{2}0\rangle$ family described by stacking of pure A or B (420) planes, there are two common symmetry elements: a (100) mirror plane (plane of the figure in Fig. 1) and an fcc translation on a (420) plane. Thus the ensemble average of any position-dependent function will be invariant to such symmetry operations, a fact that we will next introduce into our description of the $\langle 1\frac{1}{2}0\rangle$ family.

In particular, we are interested in the computation of the multisite correlation functions which, as we shall see, completely determine the free energy.[7] An n-site correlation function is defined as the ensemble average of an n-order product of spin operators $\sigma(r)$ evaluated at different lattice sites $r_1,r_2,\ldots,r_n$. Such lattice sites will define a geometrical figure which will be referred to as an n-point cluster.

Noting that the correlation functions must be invariant to translations along a vector on a (420) plane, we can designate any such correlation by the number of points n in the cluster and the (420) plane, let us say labeled p, to which the cluster is associated. In addition, an index s will be used in order to distinguish among distinct n-point clusters, e.g., nn pairs along different crystallographic directions, nn and nnn pairs, different type of triangles, etc. Thus the multisite correlation function associated to the n-point, s-type cluster at the (420) lattice plane p, will be given by

$$\xi_{n,s}(p) = \langle \sigma(r_p)\sigma(r_p + r_1^{(s)}) \cdots \sigma(r_p + r_{n-1}^{(s)}) \rangle \ , \tag{3}$$

where r_p is any representative lattice point on the (420) plane p, and where $r_1^{(s)},\ldots,r_{n-1}^{(s)}$ are $n-1$ fcc lat-

TABLE II. Definition of the multisite correlation functions. The second column gives the points of the clusters referred to Fig. 2. The columns n, s, and $M_{n,s}$ are, respectively, the number of points in the cluster, an arbitrary classification index, and the number of clusters per lattice point.

m	Cluster	n	s	$M_{n,s}$	Description
1	*A*	1	1	1	point
2	*AB*	2	1	2	
3	*AC*	2	2	2	nn pairs
4	*AD*	2	3	1	
5	*AF*	2	4	1	
6	*AA*	2	5	1	
7	*AG*	2	6	1	nnn pairs
8	*AE*	2	7	1	
9	*ABC*	3	1	2	
10	*ABD*	3	2	2	nn triangles
11	*ACD*	3	3	2	
12	*ACF*	3	4	2	
13	*AAB*	3	5	1	
14	*AAC*	3	6	1	
15	*ABG*	3	7	2	
16	*ADG*	3	8	1	nn and nnn
17	*AEF*	3	9	1	triangles
18	*ACE*	3	10	2	
19	*ADE*	3	11	1	
20	*ABB*	3	12	1	
21	*ACC*	3	13	1	
22	*ADE*	3	14	1	
23	*ABCD*	4	1	2	nn tetrahedron
24	*ABCA*	4	2	1	
25	*ABDG*	4	3	2	
26	*ACEF*	4	4	2	
27	*ACDE*	4	5	2	
28	*ACDF*	4	6	2	nn and nnn
29	*ACCF*	4	7	1	tetrahedron
30	*ABBD*	4	8	1	
31	*ACCD*	4	9	1	
32	*ABBG*	4	10	1	
33	*ACCE*	4	11	1	nn square
34	*ADEF*	4	12	1	
35	*ABBDG*	5	1	1	
36	*ACCEF*	5	2	1	
37	*ACCDE*	5	3	1	nn pyramid
38	*ACDEF*	5	4	2	
39	*ACCDF*	5	5	1	
40	*ACCDEF*	6	1	1	octahedron

tice vectors connecting the origin r_p to the $n-1$ remaining points of the s-type, n-point cluster.

After applying the (001) mirror-plane symmetry common to the A_2B_2, A_2B, and A_3B phases of the $\langle 1\frac{1}{2}0\rangle$ family, we arrive, in the O-T approximation, at the set of forty distinct correlation functions listed in Table II. These forty correlation functions are generated from the ten basic figures (last column of Table II) in which the octahedron and the tetrahedron can be decomposed.[13] The set of letters in the second column of Table II gives the vertices of the cluster in question according to the (001) projection of the fcc lattice shown in Fig. 2. Repetition of letters, such as AA in the sixth row, refer to lattice position connected by a translation $a(001)$, with a the lattice parameter. The third and fourth columns give, respectively, the number of points n in the cluster and the index s used in the present classification scheme. Finally, the parameter $M_{n,s}$ is the number of n,s clusters per lattice point.

The average value of the energy in the nn and nnn pair approximation, Eq. (2), can be written following the notation laid out in Table II,

$$\langle E\rangle = M\sum_{s=1}^{7}\epsilon_s\sum_{p}\xi_{2,s}(p) \quad , \tag{4}$$

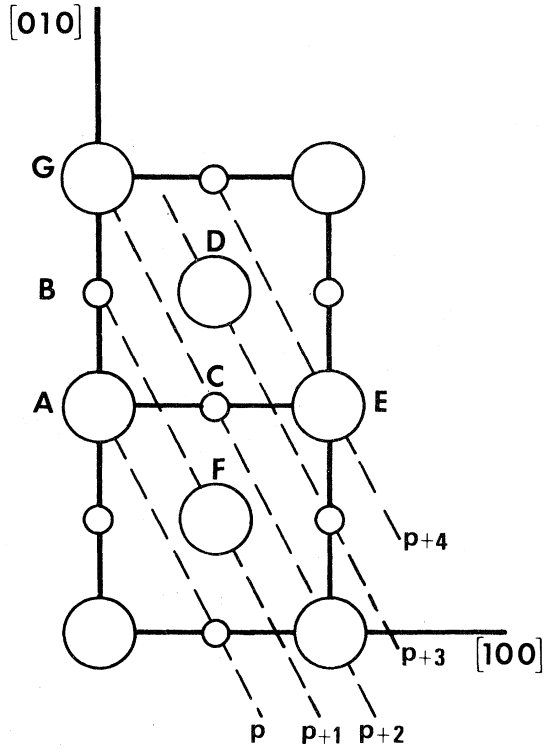

FIG. 2. Projection of the fcc lattice on a (001) plane. Traces of (420) planes are indicated by broken lines. Atoms belonging to clusters relevant to the tetrahedron-octahedron approximation are labeled $A-F$.

where M is the number of lattice points on a (420) plane and where the ϵ_s are given by

$$\epsilon_s = M_{2,s}v_1, \quad s=1,2,3,4$$

and

$$\epsilon_s = M_{2,s}v_2, \quad s=5,6,7 \quad ,$$

with v_1 and v_2 as the nn and nnn pair interaction energies, respectively. Note that since the average value of the energy depends linearly on the correlation functions $\xi_{n,s}(p)$, there is no formal distinction in the CVM between pairwise and many-body interactions. Such characteristic of the CVM can be used to closely reproduce experimental phase diagrams[3,4] without any additional difficulty. Conversely, in the process of reproducing a given phase diagram, one would hope to shed some light on the nature of the effective interactions in solid solutions.

In a given approximation of the CVM, the number of configurations Ω in Eq. (1) is written in terms of the probabilities for the different clusters to have particular arrangements or distributions of A and B atoms. Any such configuration of, let us say, the n-point, s-type cluster associated with the (420) plane p, can be designated by one of a 2^n set of n numbers $\{i,j,\ldots,k\}$ where $i,j,\ldots k$ take values $+1$ and -1 for A and B type, respectively. The probability in question will be named $x_{n,s}(i,j,\ldots k\,|p)$ or $x_{n,s}(J,p)$ where J stands for the set $\{i,j,\ldots,k\}$.

In order to write the probabilities $x_{n,s}(J,p)$ in terms of the correlations functions defined by Eq. (3), we introduce the occupation operator $\Gamma_i(r)$,[13]

$$\Gamma_i(r) = \tfrac{1}{2}[1+i\sigma(r)] \quad . \tag{5}$$

The occupation operator $\Gamma_i(r)$ takes values one if lattice point r is occupied by an i-type atom ($i=\pm1$) and zero otherwise. Thus, the probability $x_{n,s}(J,p)$ is given by

$$\begin{aligned} x_{n,s}(J,p) &\equiv x_{n,s}(i,j,\ldots,k\,|p) \\ &= \langle \Gamma_i(r_p)\Gamma_j(r_p+r_1^{(s)}\cdots\Gamma_k(r_p+r_{n-1}^{(s)}))\rangle \quad , \end{aligned} \tag{6}$$

where as before $r_1^{(s)},\ldots,r_{n-1}^{(s)}$ define the n-point, s-type cluster and r_p is a representative lattice point on the (420) plane p.

Using Eq. (5) and expanding the product of $\Gamma_i(r)$'s in Eq. (6) one can write

$$x_{n,s}(J,p) = \frac{1}{2^n}\left[1+\sum_{n'}\sum_{s'}\sum_{p'}V_{n,s;n',s'}(J,p'-p)\xi_{n',s'}(p')\right] , \tag{7}$$

where, in general, $V_{n,s;n',s'}(J,p'-p)$ is different from zero for values of $p'-p$ such that the cluster n',s'

associated with the (420) plane p' is completely contained in the cluster n,s associated with p and, in such a case, is given by a sum of n'-order products involving the indices $i,j,\ldots,k$ of configuration J.

The cluster concentrations relevant to the T-O approximation are those for the point cluster ($n=1,s=1$), the nn pairs ($n=2,s=1,2,3,4$), the nn triangle ($n=3,s=1,2,3,4$), the regular tetrahedron ($n=4,s=1$) and the octahedron ($n=6,s=1$).[13]

In terms of the correlation functions, the point and the nn pairs concentrations are explicitly given by:

$$x_{1,1}(i|p)=\tfrac{1}{2}[1+i\xi_{1,1}(k)] \tag{8a}$$

and

$$x_{2,s}(i,j|p)=\tfrac{1}{4}[1+i\xi_{1,1}(p)+j\xi_{1,1}(p+m_s)+ij\xi_{2,s}(p)]\ , \tag{8b}$$

where m_s take, respectively, values 1,2,3,1 for s equal 1,2,3,4 and where atom i is on plane p and j on plane $p+m_s$ ($i,j=\pm 1$).

Similarly, the concentration $x_{4,1}(i,j,k,l|p)$ for the regular tetrahedron with atoms i,j,k,l on planes p, $p+1$, $p+2$, and $p+3$, respectively, is given by

$$\begin{aligned}x_{4,1}(i,j,k,l|p)=\tfrac{1}{16}[&1+i\xi_{1,1}(p)+j\xi_{1,1}(p+1)+k\xi_{1,1}(p+2)+l\xi_{1,1}(p+3)\\&+ij\xi_{2,1}(p)+kl\xi_{2,1}(p+2)+ik\xi_{2,2}(p)+jl\xi_{2,2}(p+1)\\&+il\xi_{2,3}(p)+jk\xi_{2,4}(p+1)+ijk\xi_{3,1}(p)+ijl\xi_{3,2}(p)\\&+ikl\xi_{3,3}(p)+jkl\xi_{3,4}(p+1)+ijkl\xi_{4,1}(p)]\ .\end{aligned} \tag{8c}$$

TABLE III. Partial sums of Eq. (7) for the four types of nn triangles. The configuration J corresponds to a triplet of numbers i,j,k ($i,j,k=\pm 1$) occupying, respectively, planes $p,p+1,p+2$ for $s=1$; $p,p+1,p+3$ for $s=2$; $p,p+2,p+3$ for $s=3$; and $p,p+1,p+2$, for $s=4$.

n'	s	$\sum_{p'}\sum_{s'} V_{3,s;n',s'}(J,p'-p)\xi_{n',s'}(p')$
1	1	$i\xi_{1,1}(p)+j\xi_{1,1}(p+1)+k\xi_{1,1}(p+2)$
1	2	$i\xi_{1,1}(p)+j\xi_{1,1}(p+1)+k\xi_{1,1}(p+3)$
1	3	$i\xi_{1,1}(p)+j\xi_{1,1}(p+2)+k\xi_{1,1}(p+3)$
1	4	$i\xi_{1,1}(p)+j\xi_{1,1}(p+1)+k\xi_{1,1}(p+2)$
2	1	$ij\xi_{2,1}(p)+ik\xi_{2,2}(p)+jk\xi_{2,4}(p+1)$
2	2	$ij\xi_{2,1}(p)+ik\xi_{2,3}(p)+jk\xi_{2,2}(p+1)$
2	3	$ij\xi_{2,2}(p)+ik\xi_{2,3}(p)+jk\xi_{2,1}(p+2)$
2	4	$ij\xi_{2,4}(p)+ik\xi_{2,2}(p)+jk\xi_{2,1}(p+1)$
3	1	$ijk\xi_{3,1}(p)$
3	2	$ijk\xi_{3,2}(p)$
3	3	$ijk\xi_{3,3}(p)$
3	4	$ijk\xi_{3,4}(p)$

The concentration for the four types of nn triangles and for the octahedron, in terms of the forty correlation functions defined in Table II, are given in Tables III and IV.

Having characterized the concentration variables relevant to the T-O approximation, we proceed with the computation of the number of configurations Ω [Eq. (1)] which, in the disordered state, is given by[13]

$$\Omega_{\rm dis}=\frac{\{\triangle\}^8\{\cdot\}}{\{-\}^6\{\text{tet}\}^2\{\text{oct}\}}\ , \tag{9}$$

where each bracket stands for a product of factorials of the form

$$\{n\}=\prod_J Nx_n(J)!\ ,$$

with n referring to the cluster enclosed by the bracket and with N the total number of lattice points. The plane index p and the cluster-type index s has been omitted in the concentration variables for the disordered state.

TABLE IV. Partial sums of Eq. (7) for the octahedron. The configuration J corresponds to the set of numbers $i,j,k,l,m,n\,(=\pm 1)$ occupying, respectively, planes $p, p+1, p+2, p+2, p+3$, and $p+4$.

n'	$\sum_{p'}{}' \sum_{s'}{}' V_{6,1;n',s'}(J,p'-p)\,\xi_{n',s'}(p')$
1	$i\xi_{1,1}(p)+j\xi_{1,1}(p+1)+(k+l)\xi_{1,1}(p+2)+m\xi_{1,1}(p+3)+n\xi_{1,1}(p+4)$
2	$ij\xi_{2,4}(p)+i(k+l)\xi_{2,2}(p)+im\xi_{2,3}(p)+j(k+l)\xi_{2,1}(p+1)+jn\xi_{2,3}(p+1)$ $+n(k+l)\xi_{2,2}(p+2)+m(k+l)\xi_{2,1}(p+2)+mn\xi_{2,4}(p+3)$ $+in\xi_{2,7}(p)+jm\xi_{2,6}(p+1)+kl\xi_{2,5}(p+2)$
3	$ij(k+l)\xi_{3,4}(p)+im(k+l)\xi_{3,3}(p)+jn(k+l)\xi_{3,2}(p+1)+mn(k+l)\xi_{3,1}(p+2)$ $+in(k+l)\xi_{3,10}(p)+inm\xi_{3,11}(p)+ijn\xi_{3,9}(p)+ijm\xi_{3,14}(p)+ikl\xi_{3,13}(p)$ $+jm(k+l)\xi_{3,7}(p+1)+jmn\xi_{3,8}(p+1)+jkl\xi_{3,12}(p+1)+klm\xi_{3,5}(p+2)$ $+kln\xi_{3,6}(p+2)$
4	$ijn(k+l)\xi_{4,4}(p)+imn(k+l)\xi_{4,5}(p)+ijkl\xi_{4,7}(p)+iklm\xi_{4,9}(p)$ $+ijm(k+l)\xi_{4,6}(p)+jkln\xi_{4,8}(p+1)+jmm(k+l)\xi_{4,3}(p+1)+klmn\xi_{4,2}(p+2)$ $+ijmn\xi_{4,12}(p)+ikln\xi_{4,11}(p)+jklm\xi_{4,10}(p+1)$
5	$ijmn(k+l)\xi_{5,4}(p)+ijkln\xi_{5,2}(p)+iklnm\xi_{5,3}(p)+ijklm\xi_{5,5}(p)+jklmn\xi_{5,1}(p+1)$
6	$ijklmn\xi_{6,1}(p)$

In the ordered state, Eq. (9) for the number of configurations Ω is modified slightly by the fact that concentrations on different sublattices are distinguished. For the case of an ordered structure described by L distinct sublattices [(420) planes], each bracket in Eq. (9) becomes

$$\{n\}=\prod_{p=1}^{L}\prod_{s}\left[\prod_{J}(N/L)x_{n,s}(J,p)!\right]^{\alpha_{n,s}} ,$$

with the exponent $\alpha_{n,s}$ given by

$$\alpha_{n,s}=M_{n,s}/\sum_{s'}{}' M_{n,s'} ,$$

where $M_{n,s}$ is the number of clusters per lattice point, (see Table II), and where the sum in the denominator is over all s-type cluster corresponding to the n-point cluster in Eq. (9) (e.g., $s=1,2,3,4$ for the nn pairs).

Using Stirling's approximation for the logarithm of the number of configurations Ω and Eq. (4) for the average energy $\langle E\rangle$, one obtains the free energy per lattice site

$$f=\frac{F}{N}=\frac{1}{L}\sum_{p=1}^{L}\left[\sum_{s=1}^{7}\epsilon_s\xi_{2,s}(p) - k_BT\sum_{(n,s)}{}'\gamma_{n,s}f_{n,s}(p)\right] , \qquad (10)$$

where the p summation is over the L sublattices and where the sum over n,s is restricted to the point ($\gamma_{1,1}=1$), the nn pairs ($\gamma_{2,1}=\gamma_{2,2}=-2$ and $\gamma_{2,3}=\gamma_{2,4}=-1$), the nn triangles ($\gamma_{3,s}=2$ for $s=1,2,3,4$), the nn tetrahedron ($\gamma_{4,1}=-2$), and the octahedron ($\gamma_{6,1}=-1$) clusters. Finally, the functions $f_{n,s}(p)$ are given by

$$f_{n,s}(p)=\sum_{J}x_{n,s}(J,p)\ln x_{n,s}(J,p) . \qquad (11)$$

The determination of the phase diagrams for the A_2B_2, A_2B, and A_3B phases of the $\langle 1\frac{1}{2}0\rangle$ family, requiring the minimization of the free energy with respect to the multisite correlation functions, will be discussed in Sec. IV. In Sec. III, we undertake the calculation of instability temperatures in k space.

III. STABILITY ANALYSIS

The study of the stability of the disordered phase to small changes in the configurational variables such as the long-range-order parameters or more generally the multisite correlation functions $\xi_{n,s}(p)$ is of fundamental importance for the characterization of fluctuations in the disordered phase as well as for determin-

ing the critical lines associated to higher-order transitions. The concept of stability limit, coincident with the critical point in higher-order transitions, is generally extended into metastable regions (below first-order transition lines), defining the so-called ordering spinodal.[9]

Formally, the stability limit is determined by the vanishing of the second differential of the free energy

$$d^2f=\sum_{l,p}\sum_{l',p'}F_{ll'}(p,p')\,d\xi_l(p)\,d\xi_{l'}(p') \quad , \tag{12}$$

where $F_{ll'}(p,p')$ stands for the second derivatives of f with respect to $\xi_l(p)$ and $\xi_{l'}(p')$, evaluated in the disordered state, and where the indices l and l' refer to n,s and n',s', respectively.

Using Eqs. (7), (10), and (11), one obtains for the second derivatives

$$F_{ll'}(p,p')=-\frac{k_BT}{L}\sum_{p''=1}^{L}\sum_{l''}\frac{\gamma_{l''}}{2^{2n''}}\sum_{J}\frac{V_{l''l}(J,p''-p)\,V_{l''l'}(J,p''-p')}{x_{l''}(J)} \quad , \tag{13}$$

where p is omitted from the concentrations $x_{l''}(J)$ in the disordered state, and where the number of sublattices L is taken equal to the total number of (420) lattice planes in the crystal. This particular choice of sublattices reduces the problem to one dimension, although no particular difficulty would arise if each lattice point were considered as a distinct sublattice.

Noting that $F_{ll'}(p,p')$ is a function of $p-p'$ due to the translational symmetry of the disordered state [see Eq. (13)], one obtains after Fourier transforming Eq. (12)

$$d^2f=\frac{1}{L}\sum_{h}\sum_{ll'}\Phi_{ll'}(h)\,dX_l(-h)\,dX_{l'}(h) \quad ,$$

with $\Phi_{ll'}(h)$ and $X_l(h)$ the Fourier transforms, respectively, of $F_{ll'}(p-p')$ and $\xi_l(p)$ given by

$$\Phi_{ll'}(h)=\sum_{r}F_{ll'}(p)e^{i\vec{k}_h\cdot\vec{r}_p}$$

and

$$X_l(h)=\sum_{p}\xi_l(p)e^{i\vec{k}_h\cdot\vec{r}(p)} \quad ,$$

where $\vec{r}_p$ is an arbitrary vector on the (420) plane p and where the reciprocal-lattice vector $\vec{k}_h$ is given by

$$\vec{k}_h=(2\pi/a)h(2,1,0) \quad ,$$

with a the lattice parameter and $h=m/L$ for $m=\pm1,\ldots,\pm L$.

Within the level of approximation chosen, the complete thermodynamic description of the state of order is given by the minimization of the free energy [Eq. (10)] and by the analysis of the eigenvalues and eigenvectors of the Hermitian matrix $\Phi(h)$ with elements $\Phi_{ll'}(h)$. Minimization of the free-energy results in the expectation values for all the multisite correlation functions whereas from the eigenvalues and eigenvectors of $\Phi(h)$ one obtains the fluctuations in the mean-square amplitudes of the cluster correlation waves for arbitrary wave vector $\vec{k}_h$.[14]

In particular, the stability limit (second-order transition line or ordering spinodal) is given by the vanishing of the smallest eigenvalue $\lambda_m(h)$ of the matrix $\Phi(h)$. The results of the computations for the $\langle 1\frac{1}{2}0\rangle$ family (Sec. IV) show that the vanishing of $\lambda_m(h)$ takes place, as suggested by general symmetry arguments,[9] at the so-called special points of the fcc lattice.

IV. CALCULATION OF THE PHASE DIAGRAM

The calculation of the equilibrium phase diagram requires the minimization of the free-energy subject to the constraint of constant concentrations of A and B atoms. This is realized by minimizing the grand potential

$$g=f+(\mu/L)\sum_{p=1}^{L}\xi_{1,1}(p) \quad , \tag{14}$$

where $\xi_{1,1}(p)$ is, according to Table II, the point correlation function on sublattice p and where μ is the appropriate chemical potential.

By using Eqs. (10) and (14) one obtains the following set of nonlinear algebraic equations describing the equilibrium condition for each phase:

$$\frac{\partial g}{\partial\xi_{n,s}(p)}=0=\frac{1}{L}\left[\epsilon_s\delta_{n,2}+\mu\delta_{n,1}-k_BT\sum_{n'}\sum_{s'}\sum_{p'}\frac{\gamma_{n',s'}}{2^{n'}}\sum_{J}V_{n',s';n,s}(J,p-p')\ln x_{n',s'}(J,p')\right] \quad , \tag{15}$$

where $\delta_{n,n'}$ takes value one for $n=n'$ and zero otherwise.

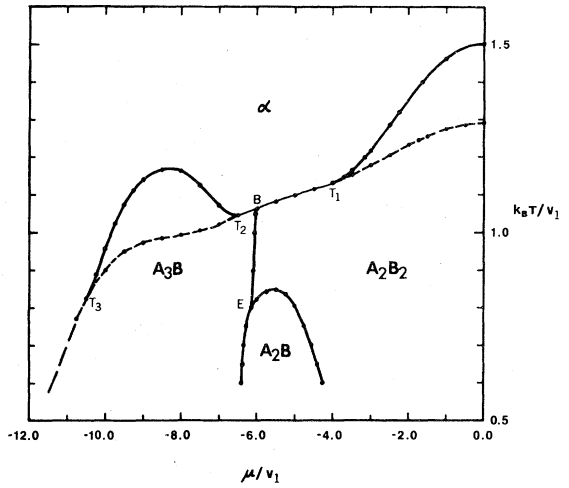

FIG. 3. Temperature vs chemical potential phase diagram for the $\langle 1\frac{1}{2}0\rangle$ family of ordered superstructures. The phase diagram was calculated for a ratio of second to first-neighbor interactions energies of 0.25. Dots represent calculated points.

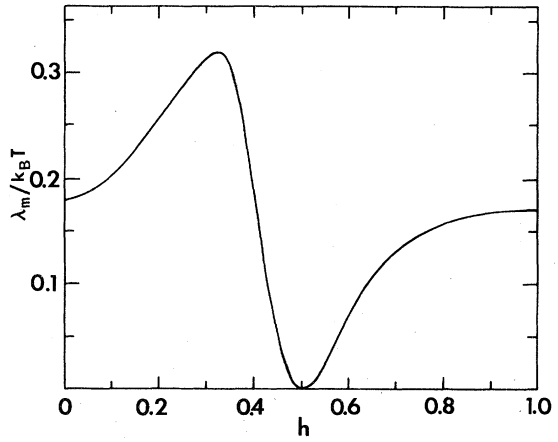

FIG. 4. Smallest eigenvalue of the matrix of second derivatives of the free energy along the (210) direction in reciprocal space. For the values of chemical potential ($\mu=-3v_1$) and temperature ($T=1.2v_1$) chosen, the smallest eigenvalue is seen to vanish at $h=0.5$ indicating a $\langle 1\frac{1}{2}0\rangle$ instability.

The system of equations (15) was solved in each phase for different set of values of the chemical potential μ and the reduced temperature $\tau=k_BT/v_1(v_1>0)$, and for a ratio of nnn to nn interaction energies v_2/v_1 of 0.25. This particular ratio of pair interaction energies was chosen in order to fall within the range 0 to $\frac{1}{2}$ where the ordered superstructures of the $\langle 1\frac{1}{2}0\rangle$ family are known to be ground states.

Finally the coexistence lines for the different phases in the (μ,T) phase diagram are determined from the point of intersection of the associated grand potentials. The complete (μ,T) phase diagram, including the ordering spinodal (dotted line) is shown in Fig. 3. In what follows, a brief description of the calculations for each phase is given.

A. Disordered state

The set of distinct correlation functions in the disordered state is obtained by noting that all (420) planes are equivalent (fcc translational symmetry) and that different variants of a given cluster, e.g., $s=1,2,3,4$ for nn pairs, are indistinguishable (point group symmetry of the fcc lattice). We arrive in this way at ten correlation functions associated with each of the clusters listed in the last column of Table II. Consequently, the minimization conditions, Eq. (15), reduce to a set of ten algebraic equations. These equations were solved (using the Newton-Raphson iteration scheme) in order to obtain the grand potential and the equilibrium values of the cluster probabilities. With the latter, the smallest eigenvalue $\lambda_m(h)$ of the matrix of the Fourier transform of the second derivatives of the free energy was calculated (see Sec. III). Figure 4 shows a plot of $\lambda_m(h)$ vs h ($\langle 1\frac{1}{2}0\rangle$ direction in reciprocal space) for $\mu=-3.0v_1$ and $k_BT=1.2v_1$. Since λ_m vanishes at $h=0.5$, the particular values of chemical potential and temperature chosen correspond to the stability limit or ordering spinodal. The point in k space at which λ_m first vanishes was found to be, for all values of chemical potential, the fcc special point $\langle 1\frac{1}{2}0\rangle(h=0.5)$ in agreement with general symmetry arguments.[9] The complete $\langle 1\frac{1}{2}0\rangle$ ordering spinodal is shown in dashed lines in the (μ,T) phase diagram of Fig. 3.

B. A_2B_2 phase

Figure 1(a) shows the four sublattices ($p=1,2,3,4$) needed for the description of the A_2B_2 ordered phase ($I4_1/amd$). With the forty correlation functions per lattice plane listed in Table II, one obtains a set of 160 such correlations which, however, are not all distinct due to the symmetry elements of the associated point group. In addition to the (001) mirror symmetry (used in the definitions of Table II), the A_2B_2 structure is invariant to a fourfold roto-inversion [(010) axis], an inversion through $(\frac{1}{4},\frac{3}{4},0)$ (and equivalent points) and a reflection through the (100) plane. Application of such symmetry operations to the minimization of the free-energy results in 33 nonlinear equations in as many independent variables (correlation functions).

A plot of the grand potential for the disordered and the A_2B_2 phases vs reduced temperatures $\tau=k_BT/v_1$

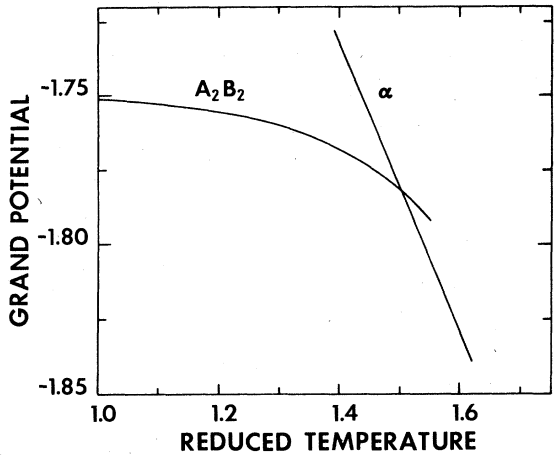

FIG. 5. Grand potential vs temperature for the A_2B_2 and disordered (α) phases for zero chemical potential. The intersection of grand potentials gives the values of temperature and chemical potential at which both phases coexist.

and for zero chemical potential is shown in Fig. 5. The transition, taking place at $\tau \simeq 1.501$, is strongly first order as indicated by the plot of long-range-order parameter η (Fig. 6), with η given by

$$\eta = \tfrac{1}{4}[\xi_{1,1}(1) + \xi_{1,1}(2) - \xi_{1,1}(3) - \xi_{1,1}(4)] \ .$$

The line of first-order transitions (for $\mu = 0$ to $\mu \simeq -3.9v_1$) joins the ordering spinodal, which becomes a critical line, at the tricritical point[14] T_1 approximately given by $\mu = -3.9v_1$ and $k_B T \simeq 1.13v_1$ (see Fig. 3). The higher-order character of the transition for larger absolute values of the chemical potential is illustrated in Fig. 7 by the plot of long-range-order parameter versus temperature for $\mu = -5.0v_1$.

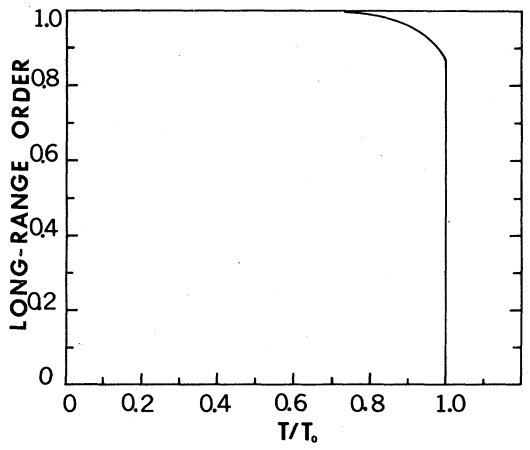

FIG. 6. Long-range-order parameter for the A_2B_2 phase as a function of temperature for zero chemical potential.

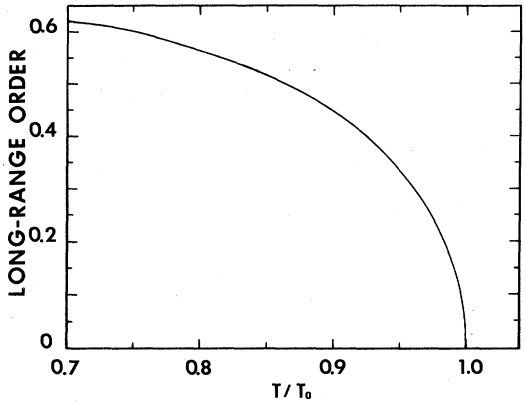

FIG. 7. Long-range-order parameter for the A_2B_2 phase as a function of temperature for chemical potential equal to $-5.0v_1$.

C. A_3B phase

The symmetry elements of the $D0_{22}$ structure ($I4/mmm$) are the three mirror planes (001), (010), and (100); a center of inversion [0 in Fig. 1(c)], a fourfold axis [(010)], and a fourfold roto-inversion axis [dotted (010) axis in Fig. 1(c)]. Combining these symmetry operations with the definitions of Table II and the four sublattices in Fig. 1(c) we arrive at a set of 45 distinct correlation functions for the A_3B phase.

The disorder to A_3B transformation is first order near stochiometry (for values of μ between -6.5 and $-10.5v_1$, approximately) becoming a higher-order transition at the tricritical points T_2 and T_3 (see Fig. 3). Typical plots of the long-range-order parameters versus temperature for first- and second-order transitions are shown in Figs. 8 and 9 for $\mu = -8.5v_1$ and $\mu = -6.5v_1$, respectively. The two long-range-order parameters in both, Fig. 8 and Fig. 9, correspond to the amplitude of the $\langle 100 \rangle$ and $\langle 1\tfrac{1}{2}0 \rangle$ concentration waves describing the $D0_{22}$ structure,[9] and in terms of the point correlation functions are given by

$$\eta_{100} = \tfrac{1}{2}[\,\xi_{1,1}(1) - \xi_{1,1}(2) + \xi_{1,1}(3) - \xi_{1,1}(4)\,]$$

and

$$\eta_{1\frac{1}{2}0} = \tfrac{1}{2}[\,\xi_{1,1}(1) + \xi_{1,1}(2) - \xi_{1,1}(3) - \xi_{1,1}(4)\,] \ .$$

The line of first-order transitions for the reaction $A_3B \rightarrow A_2B_2$ runs almost vertically in the phase diagram of Fig. 3 meeting, at high temperatures, the two critical lines at the bicritical point[15,16] B. At lower temperatures, the line of first-order transition ends at the triple point E, where the A_2B_2, A_2B, and A_3B phases coexist.

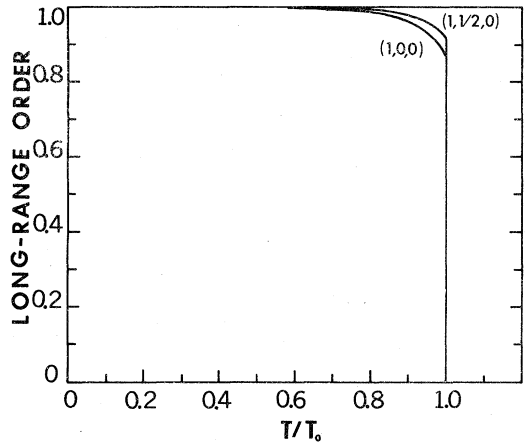

FIG. 8. Long-range-order parameters for the A_3B phase as a function of temperature for $\mu=-8.5v_1$. The order parameters correspond to the amplitude of the point correlation waves of wave vector (100) and $(1,\frac{1}{2},0)$ which describe the $D0_{22}$ structure.

D. A_2B phase

The relevant symmetry operations for the A_2B phase ($Immm$) are the three mirror planes (001), (110), and $(\bar{1}10)$ and a center of inversion [0 in Fig. 1(b)]. From the 40 correlation functions per (420) plane listed in Table II and the three sublattices shown in Fig. 1(b), one obtains, after applying the symmetry operations, a set of 46 distinct correlation functions.

The narrow A_2B phase field is seen to appear at relatively low temperatures (Fig. 3), the most salient feature being the triple point E at approximately $\mu=-6.1v_1$ and $k_BT=0.8v_1$.

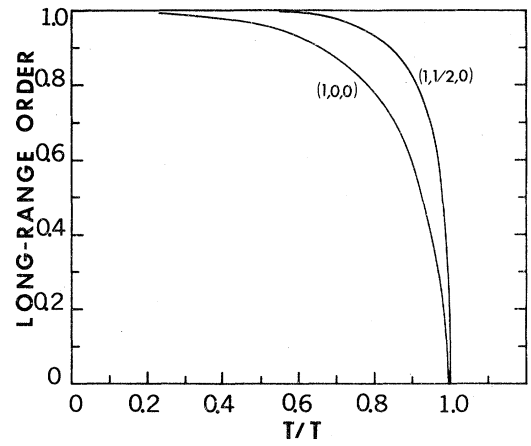

FIG. 9. Long-range-order parameters shown in Fig. 8 for the A_3B phase are plotted for $\mu=-6.5v_1$. For this value of chemical potential the transition is second order.

E. A_4B phase

We investigated the A_4B structure which, although not a ground state in the nn and nnn pair approximation, appears to be closely related to the other structures of the $\langle 1\frac{1}{2}0\rangle$ family. The $D1_a$ structure ($I4/m$) has, in addition to the (001) mirror symmetry, a fourfold (001) symmetry axis. Combining these symmetry operations, Table II and the five sublattices of Fig. 1(d), one arrives at 57 distinct correlation functions.

The grand potential for the A_4B phase was calculated for values of the reduced temperatures higher than 0.55 and chemical potentials in the neighborhood of $-10v_1$. In this temperature range, the A_4B phase was found to be unstable, as illustrated in Fig. 10 by the comparison of grand potentials of A_3B and A_4B phases at $\tau=0.8$. Note that although the A_4B phase may become stable with respect to A_3B at sufficiently low temperatures ($\tau<0.55$), one would expect that it will remain unstable with respect to the monoclinic A_5B structure mentioned in the Introduction. This latter phase, however, will not be considered in this investigation.

Finally, Fig. 11 shows the composition versus reduced temperature phase diagram corresponding to the (μ,T) diagram of Fig. 3, for the concentration range 0.1 to 0.5 and reduced temperature range 0.5 to 1.6.

V. DISCUSSION

A prototype order-disorder phase diagram for the $\langle 1\frac{1}{2}0\rangle$ family has been calculated in the T-O approximation of the CVM. Two features of this approxima-

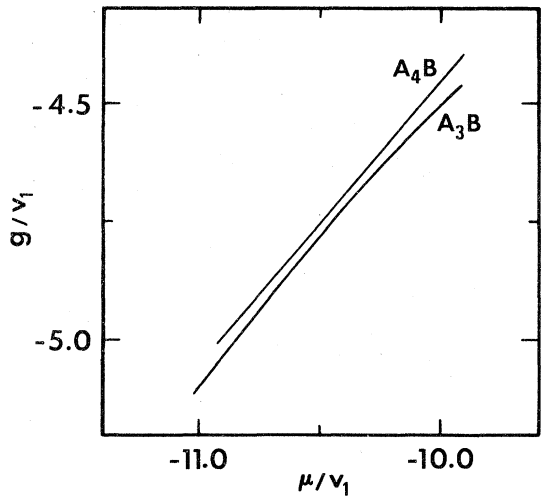

FIG. 10. Grand potential vs chemical potential for the A_3B and A_4B phases for k_BT equal to $0.8v_1$.

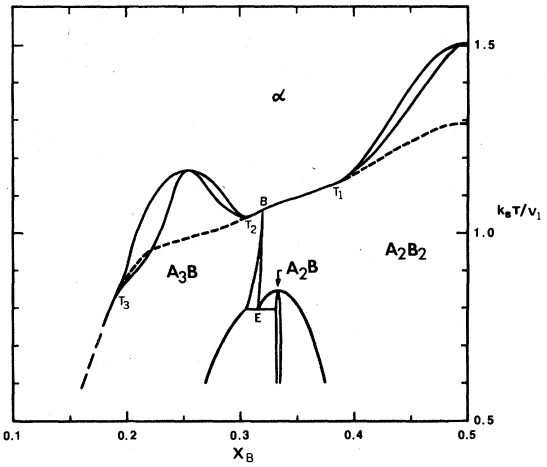

FIG. 11. Temperature-composition phase diagram corresponding to the (μ, T) diagram of Fig. 3.

tion make the calculation particularly attractive: first, the numerical results appear to be very reliable, as previous calculations of the critical temperature for the spin-$\frac{1}{2}$ Ising model have shown,[11,12] and second, nn and nnn pair interactions can be included in the configurational energy. Both types of interactions (nn and nnn pairs) are essential for the ordered superstructures of the $\langle 1\frac{1}{2}0\rangle$ family to be ground states.

Since most ordered superstructures in the fcc lattice can be shown to be ground states on the basis of nn and nnn interactions only, the *T-O* approximation should prove applicable to a large number of ordering systems. Some characteristics of the phase diagrams of real systems, such as asymmetry in the exchange of *A* and *B* atoms, cannot be accounted for by a simple pair interaction energy. Such features, however, can be reproduced very closely through the use of many-body interactions, a point clearly illustrated by recent calculations in the CuAu system.[3,4] In this respect, the CVM is very attractive since many-body interactions do not present any additional formal or computational difficulties. In the *T-O* approximation, seven many-body interactions (triangle, square, tetrahedron, ..., octahedron) may be varied continuously. It is then clearly impractical to derive complete "global" phase diagrams with all of these parameters plus the two pair interactions plus the chemical potential as independents variables. Rather we plan to vary some of these parameters within restricted ranges of values in order to see how calculated phase diagrams may approach those real systems such as Ni-Mo, Ni-V, Au-Cr, etc. First, the influences of many-body interactions on the ground states of order must be investigated, a study which is now under way.

In order to determine the equilibrium free energy in the *T-O* approximation, one must solve systems of simultaneous nonlinear algebraic equation in 50 or more independent variable. The problem can be handled very efficiently with the Newton-Raphson method. It should be pointed out, however, that the initial values at the onset of the interations are very critical: if the chosen initial values are not close to the correct equilibrium ones, the algorithm rapidly produces values of the correlation functions ξ which fall outside of a convex polyhedral region in multidimensional configuration space defined by the set of inequalities

$$x_{n,s}(J,p) \geq 0 \ ,$$

with cluster concentration x expressed linearly as a function of the ξ variables by Eq. (7). Any acceptable state of order may be described by a vector $\vec{\xi}$ the end point of which must lie entirely within the convex configuration polyhedron.[17] The vertices of the configuration polyhedron correspond to states of perfect order.

The characterization of the state of order achieved by the CVM calculations is very complete: long- and short-range-order parameters (in the form of linear combinations of correlation functions) as well as the cluster probabilities for all clusters involved are obtained immediately as a result of the free-energy minimization. Additionally, the treatment of instabilities presented in Sec. III allows the study of ordering instabilities (spinodals) and of fluctuations in reciprocal space.

ACKNOWLEDGMENTS

The authors wish to acknowledge many helpful discussions with Dr. Ryoichi Kikuchi. This investigation was supported by the Army Research Office (Durham).

*Present address: Dept. of Mater. Sci., Univ. of Calif., Berkeley, Calif. 94720.

[1]R. Kikuchi, Phys. Rev. B 81, 988 (1951).
[2]C. M. Van Baal, Physica (Utrecht) 64, 571 (1973).
[3]D. de Fontaine and R. Kikuchi, NBS Publication SP-496, 999 (1978) (unpublished).
[4]R. Kikuchi and D. de Fontaine, NBS Publication SP-496, 967 (1978) (unpublished).
[5]M. S. Richards and J. W. Cahn, Acta Metall. 19, 1263 (1971).
[6]S. M. Allen and J. W. Cahn, Acta Metall. 20, 423 (1972).
[7]J. Kanamori and Y. Kakehashi, J. Phys. (Paris) 38, Suppl. C7-274 (1978).
[8]J. W. Cahn and R. Kikuchi, Acta Metall. (to be published).

[9]D. de Fontaine, Acta Metall. 23, 553 (1975).
[10]D. de Fontaine, in *Solid State Physics,* edited by H. Ehrenreich, F. Seitz, and D. Turnbull (Academic, New York, 1979), Vol. 34, p. 73.
[11]P. R. Okamoto and G. Thomas, Acta Metall. 19, 825 (1971).
[12]S. K. Aggarwal and T. Tanaka, Phys. Rev. B 16, 3963 (1977).
[13]J. M. Sanchez and D. de Fontaine, Phys. Rev. B 17, 2926 (1978).
[14]See for example, L. D. Landau and E. M. Lifshitz, *Statistical Physics* (Addison-Wesley, Reading, Mass., 1958).
[15]R. B. Griffiths, Phys. Rev. B 7, 545 (1973).
[16]M. E. Fisher and D. R. Nelson, Phys. Rev. Lett. 32, 1350 (1974).
[17]T. Kudō and S. Katsura, Prog. Theor. Phys. 56, 435 (1976).